IBRACON Structures and Materials Journal
Revista IBRACON de Estruturas e Materiais

ORIGINAL ARTICLE

Numerical-experimental study of neighboring wind effects on tall buildings related to serviceability via reliability

Estudo numérico-experimental do efeito de vizinhança em edifícios altos devido ao vento relacionado ao desempenho via confiabilidade

Matheus Nunes Reis[a]
Thiarly Feitosa Afonso de Lavôr[a]
João da Costa Pantoja[b]
José Luís Vital de Brito[a]

[a]Universidade de Brasília – UnB, Departamento de Engenharia Civil e Ambiental, Brasília, DF, Brasil
[b]Universidade de Brasília – UnB, Departamento de Tecnologia, Brasília, DF, Brasil

Abstract: In this paper a reliability analysis was carried out, regarding the dynamic responses of displacements and accelerations in the x and y directions at the top of CAARC standard tall building, determined by the numerical-experimental High Frequency Pressure Integration technique (HFPI). The building was studied on distinct angles, subjected to dynamic wind load, isolated and with the presence of different neighbors. Tendency curves and its equations for reliability indices and maximum responses, in relation to the directions adopted to the CAARC, were presented. With the results found, it was noticed that the existence of neighborhood affects the responses of maximums and the reliability indexes, both for increase and decrease compared to the isolated building, depending on the situation and the type of dynamic response.

Keywords: neighboring wind effect, CAARC standard tall building, reliability analysis, serviceability limit states, wind tunnel.

Resumo: Neste artigo foi realizada análise de confiabilidade referente às respostas dinâmicas de deslocamentos e acelerações nas direções x e y no topo do CAARC standard tall building, determinadas com a técnica numérica-experimental High Frequency Pressure Integration (HFPI). A edificação foi estudada em distintos ângulos, submetida à carga dinâmica de vento, isoladamente e com existência de diferentes vizinhanças. Foram apresentadas curvas de tendências e suas equações para índices de confiabilidade e respostas de máximos, em relação às direções adotadas ao CAARC. Com os resultados encontrados observou-se que a existência de vizinhança afeta as respostas de máximos e os índices de confiabilidade, tanto para aumento quanto para redução em comparação com a edificação isolada, a depender da situação e do tipo de resposta dinâmica.

Palavras-chave: efeito de vizinhança, edifício alto padrão CAARC, análise de confiabilidade, estados limites de serviço, túnel de vento.

1 INTRODUCTION

The demand for more space and the efficient use of more materials has induced the construction of higher and slimmer buildings, which are even more sensitive to wind actions. Thus, it is important to study the relation between the wind and these types of structures (Mendis et al. [1], Barile et al. [2], Bashor et al. [3] and Rist and Svensson [4]).

Analyses in terms of displacements and accelerations are the most common forms to examine dynamically the serviceability limit states of structures. Besides being able to cause harm to nonstructural walls and partitions, window and door frames, and cladding, these dynamic responses have direct influence on the productivity and the well-being of users in the buildings (Tapajós et al. [5], Lamb et al. [6], Kwok et al. [7], Burton et al. [8], Lamb and Kwok [9]).

With the raise of neighborhoods, determined by the sort of arrangement, wind protection effects or even more motions can be generated in a pre-existing building due to reconfiguration of the wind flow (Blessmann [10], [11], Blessmann and Riera [12], [13]). Studies have shown, with use of reduced scale models in wind tunnel, such as Yu et al. [14], Hui et al. [15], Fontoura [16], Kim et al. [17], [18], Vieira et al. [19], [20], Lavôr [21], among others, that the presence of buildings in the neighboring regions results in modifications of wind forces, pressures and aerodynamic coefficients.

In investigations of phenomena that has some degree of randomness, like accelerations and displacements provoked in the structures by wind loads, it is interesting to examine the variables in a probabilistic form. For this, reliability analysis can be performed, being an option of methodology for civil engineering studies ([2], Smith and Caracoglia [22], Ferreira et al. [23], Pantoja [24]).

In this paper, serviceability analyses were realized via reliability in relation to the acceleration and displacement responses in x and y directions at the top of the CAARC standard tall building, which was studied at various positions, isolated and with neighbors, under wind loads. The representation of these loads was made from wind tunnel simulations. Trend curves, and their equations, for maxima and reliability related to the dynamic responses were presented, portraying together the neighboring effects.

2 METHODOLOGY

The experiments were carried out by Lavôr, during the production of his study [21], in the wind tunnel of limited atmospheric layer, Joaquim Blessmann, of the Construction Aerodynamics Laboratory (LAC) of the Rio Grande do Sul Federal University (UFRGS). The High Frequency Pressure Integration (HFPI) technique was applied, considering the reduced model of the CAARC standard tall building. With this technique, from the instantaneous pressures experimentally determined along the perimeter of the model, displacements and accelerations at the top of the building in the x and y directions were numerically obtained. These values were compared with Brazilian and international limit criteria through reliability analysis.

For the reliability analysis, probability density functions, necessary for the application of limit state functions, associated with each type and direction of the dynamic responses were determined. The parameters of these density functions were estimated with the use of maximum likelihood, except for the standard deviation in the normal distribution, which was estimated by the square root of the unbiased estimate of variance. In this study, only cases with probability density functions approved by the chi-square goodness-of-fit test and/or by the Kolmogorov-Smirnov goodness-of-fit test were analyzed.

With limit state functions modeling, considering excessive displacements and accelerations as the failure modes, the reliability indexes, associated with the limit criteria, were established, both for the isolated model and the situations with neighborhood. These indices were evaluated in relation to the target reliability index.

Lastly, to determine the parameters of the regression equations the method of least squares was used, and the adequacy of least-squares fits was evaluated with the use of the coefficient of determination R^2.

2.1 Characterization of the simulated wind

The properties associated with the wind test profile type are shown in Figure 1.
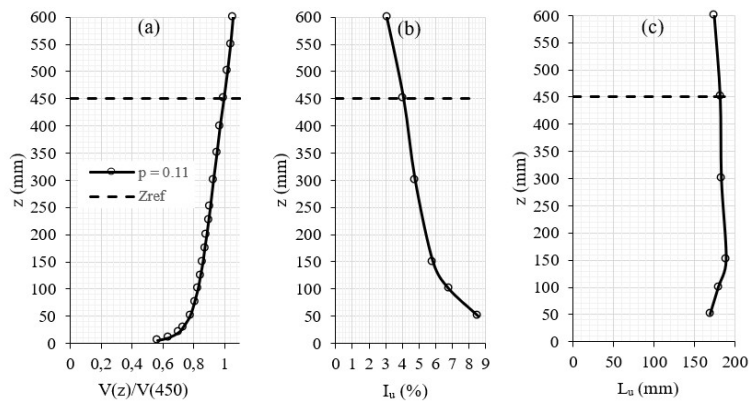
Figure 1. Characteristics of wind in tunnel tests: (a) mean wind speed profile; (b) intensity of the longitudinal turbulence component; and (c) longitudinal turbulence scale.

In Figure 1, Zref is the reference height of 450 mm referring to the top of the standard reduced model employed, $V(z)/V(450)$ is the profile of mean velocities at height z relative to Zref, I_u is intensity of the longitudinal turbulence component, and L_u is the longitudinal turbulence scale. The wind profile of exponent p at the value of 0.11, relative to large smooth surfaces more than 5 km in length, according to Category I of Terrain Roughness in NBR 6123 [25], is associated by the power law of Equation 1 (Blessmann [26]):

$$\frac{V(z)}{V(450)} = \left(\frac{z}{Zref}\right)^p \tag{1}$$

The basic wind speed V_0 was adopted equal to 50 m/s, the highest defined in the Brazilian standard isopleths [25]. The time interval of the acquisition in the wind tunnel corresponds in real structure to 600 seconds. The 1-year return period was used in the analyses performed in this work, in addition to the consideration of flat or slightly hilly terrain.

2.2 CAARC standard tall building

A CAARC Standard Tall Building specification was developed after meeting of the Commonwealth Advisory Aeronautical Research Council Coordinators in the Field of Aerodynamics, in 1969, to enable analogies of procedures applied, and data acquired, in wind tunnels (Melbourne [27]). Figure 2 depicts the standardized CAARC full-scale building with the arrangement of the 280 pressure plug indicators, in which the base center coincides with the building's vertical axis. More details can be seen in [19] and [20].
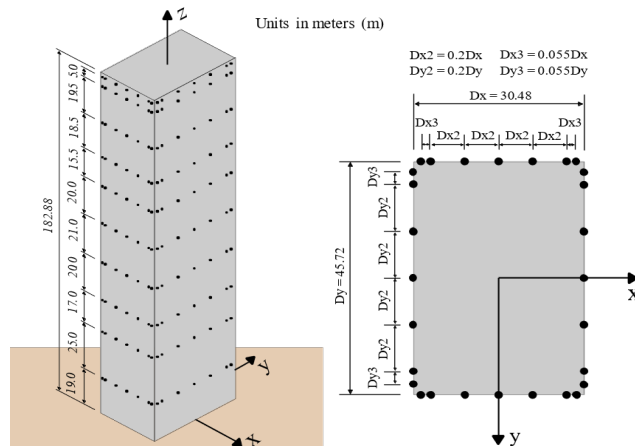

Figure 2. CAARC standard full-scale tall building and positions of the pressure plug indicators (adapted from [21]).

The building has a flat horizontal roof without parapet, with smooth facades and no geometric particularities, and dimensions of 100 ft x 150 ft x 600 ft (base dimensions and height), equivalent to 30.48 m x 45.72 m x 182.88 m [27]. The applied scale model has dimensions of 112.5 mm x 75 mm x 450 mm, for a dimension scale of 1:406.4 [21].

The CAARC model simulates a full-scale building with fundamental natural frequency f of 0.2 Hz relative to the x and y axes, shown in Figure 2, density of 160 kg/m³ and a critical damping ratio of 1% ([21], [27], Sartori [28]), which is recommended for serviceability analysis of reinforced concrete buildings [21].

2.3 Positioning of the experimental models

By means of plan view, Figure 3 shows the configurations tested in the wind tunnel. The CAARC model was rotated from 0° to 90° every 15° for each configuration: isolated (Figure 3a), with the 0° neighbor at position 3b and later at 6b (Figure 3b), and with the 90° neighbor at the same distances (Figure 3c). The presence of only one neighbor per trial, at each position and direction, was considered. The neighbor model has no pressure plugs and has identical dimensions to the CAARC.
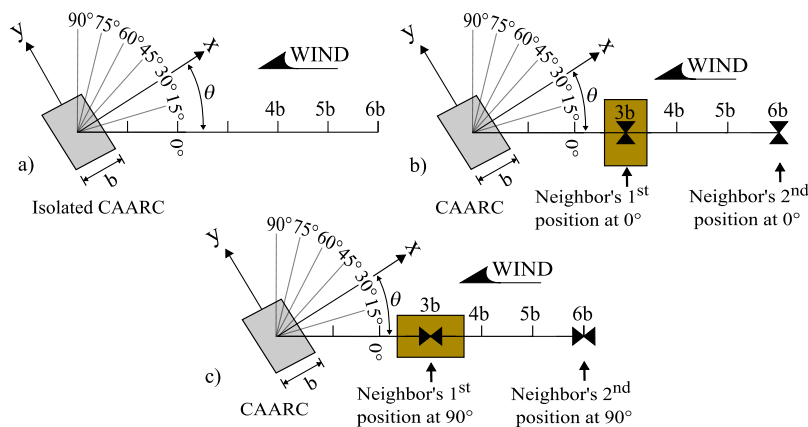

Figure 3. Top view of wind direction, neighbor's configurations and CAARC orientation angles θ, for the cases: a) isolated; b) with neighbor at 0°; and c) with neighbor at 90°.

In Figure 3, θ is the CAARC orientation angle relative to the wind direction and b is the smallest dimension of the base. In this paper, the x-direction is always related to the response perpendicular to the longest facade at the top of the CAARC, and the y-direction is always related to the response perpendicular to the shortest facade, also at the top. Figure 4 shows an example of a three-dimensional visualization of the CAARC rotated 90° with a neighbor at 0° positioned at 6b.
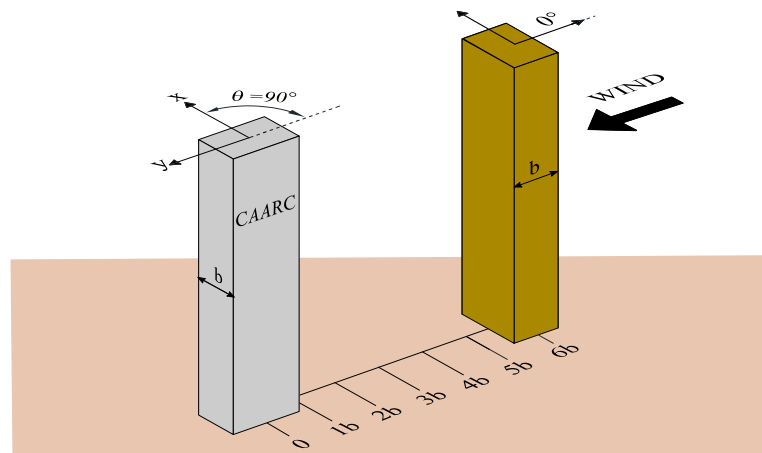

Figure 4. Three-dimensional view example with CAARC orientation angle $\theta = 90°$ and neighbor at position 6b at 0°.

Rev. IBRACON Estrut. Mater., vol. 15, no. 5, e15507, 2022

4/16

2.4 The High Frequency Pressure Integration method

In this method, the rigid experimental model was submitted to wind actions in wind tunnel for determination of the acting pressures on the facades along the time, measured by the electronic transducers. The acting forces were determined numerically by pressure integration, and the dynamic responses were defined from these forces by the numerical mode-superposition method.

Each test in the wind tunnel was executed in a period of 16 seconds, with pressure records in each plug every 0.001953 seconds, that is, with an acquisition frequency of 512 Hz, for adequate temporal representation of the wind flow and dynamic responses, totaling 8192 records in each pressure plug per experiment [21]. The adopted period corresponds to a time interval of 600 s in the real structure. In the High Frequency Pressure Integration (HFPI) technique, the pressures experimentally measured in the 16 s, related to the influence areas A (m²) of the pressure plugs, were numerically converted into forces by integration, according to Equation 2 ([21] and [28]):

$$P(t) = \int_S \left[\vec{p}(t) \, \vec{u}_F \right] dA \cong \sum_{i=1}^{n_t} \left[\vec{p}_i(t) \vec{u}_F \right] A_i \tag{2}$$

being t the time (seconds), $\vec{p}(t)$ are the local pressures (N/m²) in region s equivalent to the desired story; $\vec{p}_i(t)$ and A_i are the pressures (N/m²) and the area of influence (m²) for the i th plug, respectively; n_t is the number of plugs in the region (story) where the acting forces $P(t)$ are required, in Newtons; and $\vec{u}_F$ are direction cosines associated with the direction in which these forces are required.

With the forces determined, the dynamic responses were found from the mode-superposition method, as mentioned in [21] and [28]. In this method, according to Clough and Penzien [29], the set of displacement responses at each instant t of a multi-degree-of-freedom system, represented by the dynamic equilibrium of Equation 3, can be defined by the superposition of effects of the solutions of single-degree-of-freedom equations, each one associated with a mode of vibration n, in the form of Equation 4. The accelerations over time were determined as a function of the displacement results.

$$M \ddot{\vec{v}}(t) + C \dot{\vec{v}}(t) + K \vec{v}(t) = \vec{P}(t) \tag{3}$$

$$\ddot{Y}_n(t) + 2\xi_n \omega_n \dot{Y}_n(t) + \omega_n^2 Y_n(t) = \frac{P_n(t)}{M_n} \tag{4}$$

where $\ddot{\vec{v}}(t)$, $\dot{\vec{v}}(t)$ e $\vec{v}(t)$ are vectors of acceleration (m/s²), velocity (m/s) and displacement (in meter), respectively; M is the mass matrix (Ns²/m); C is the damping coefficients matrix (Ns/m), which constitutes the Rayleigh damping; K is the stiffness matrix (N/m); $\vec{\phi}_n$ is the mode-shape vector; $Y_n(t)$ is the modal amplitude (m), associated with its derivatives $\dot{Y}_n(t)$ (m/s) and $\ddot{Y}_n(t)$ (m/s²); $\xi_n = \vec{\phi}_n^T C \vec{\phi}_n / 2\omega_n M_n$ = critical damping ratio for the n th mode of vibration; $\omega_n = 2\pi f_n$ = natural circular frequency of the mode of vibration n (rad/s); $M_n = \vec{\phi}_n^T M \vec{\phi}_n$ = modal mass (Ns²/m); and $P_n(t) = \vec{\phi}_n^T \vec{P}(t)$ = modal force (N).

Three degrees of freedom per floor were considered in the implementation of HFPI, being rotations in relation to the x, y and z axes, as shown in Figure 2. Moreover, the modes of vibration in relation to the x and y axes were considered linear, rotating around a point at the base center of the model, and constant throughout the building axis z. It is noteworthy that this paper only presents results at the top referring to the x and y directions.

The maximum values of acceleration (m/s²) or displacement (m) responses, X_{max}, associated to the x or y direction, were estimated through the probabilistic theories of Davenport [30], applied in the Equation 5 the peak factor $\bar{\eta}_{max}$, stipulated through Equation 6.

$$X_{max} = \overline{X} + \overline{\eta}_{max}\, \sigma_X \tag{5}$$

$$\overline{\eta}_{max} = \sqrt{(2\ \ln \nu T)} + 0.5772 / \sqrt{(2\ \ln \nu T)} \tag{6}$$

where $\overline{X}$ and σ_X, respectively, are the mean and standard deviation of acceleration (m/s^2) or displacement (m) in a given direction; ν is the frequency (Hz) at which most of the spectrum energy is found, considered in this paper to be the natural frequency f; and T is the period used for calculating the average wind velocity, in seconds. The peak factor stipulated for this work was approximately 3.281.

2.5 Probabilistic analysis of the serviceability limit states

In this paper, the randomness came only from the wind actions, as the properties of the studied building were considered deterministic. All uncertainties related to wind actions were contained in the sets of pressures measured in the wind tunnel, giving rise to random dynamic responses of accelerations and displacements, obtained by using the HFPI. Uncertainty of structural responses induced by random wind actions can be better analyzed through reliability. For this purpose, the scheme shown in Figure 5 was used.
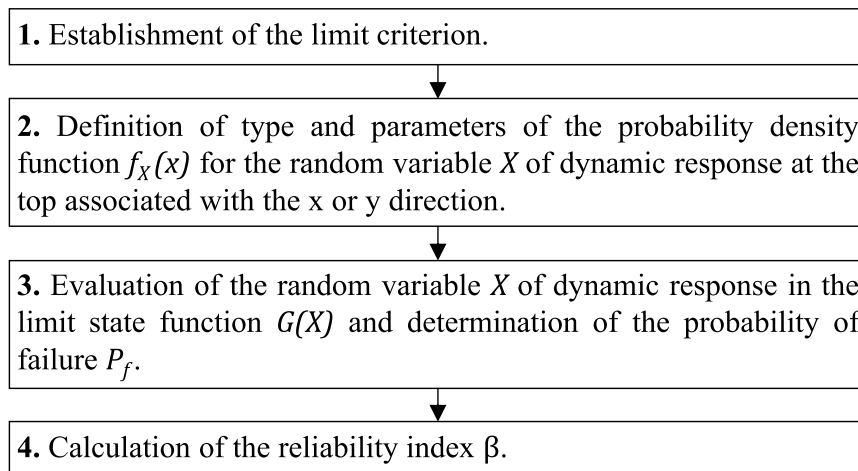
1. Establishment of the limit criterion.

2. Definition of type and parameters of the probability density function $f_X(x)$ for the random variable X of dynamic response at the top associated with the x or y direction.

3. Evaluation of the random variable X of dynamic response in the limit state function $G(X)$ and determination of the probability of failure P_f.

4. Calculation of the reliability index β.

Figure 5. Scheme used to calculate reliability index β.

As presented in Figure 5, once a limit criterion was established and considering the random variable X of displacements or accelerations at the top, for x or y direction, related to some predefined probability density function $f_X(x)$, it was possible to evaluate the random variable of dynamic response in the limit state function $G(X)$. Thus, the probability of failure P_f was determined and the corresponding reliability index β was calculated. This scheme was carried out for various situations studied, considering each type and direction of dynamic response, each one related to a probability density function and a limit criterion.

To perform the reliability analyses it was necessary to define probability density functions for the random variables. In this study, to analyze accelerations and displacements in each direction of the simulated cases, only the cases with a probability density function approved by the chi-square goodness-of-fit test and/or by the Kolmogorov-Smirnov goodness-of-fit test were considered, at the 0.05 significance level.

For the test cases with approved probability density functions, all acceleration responses were best defined by the normal distribution. However, in the isolated CAARC cases for $\theta = 0°$ and $\theta = 75°$ the displacements, in the x and y directions respectively, were defined by the beta distribution, while for $\theta = 30°$ the displacements in the x direction were best defined by the gamma distribution. In all other cases with approved probability density functions, the normal distributions were best fitted to the displacement responses.

In a reliability study, the failure domain is defined by $G(X) < 0$, while $G(X) > 0$ is the safe domain and $G(X) = 0$ is the boundary separating the previous domains. In this paper, the failure domain was considered for $G(X) \leq 0$, and Equations 7 to 10 present the limit state functions applied for the serviceability verifications.

$$G_1(\delta_x) = \delta_{lim} - |\delta_x| \tag{7}$$

$$G_2(a_x) = a_{lim} - |a_x| \tag{8}$$

$$G_3(\delta_y) = \delta_{lim} - |\delta_y| \tag{9}$$

$$G_4(a_y) = a_{lim} - |a_y| \tag{10}$$

where δ_x and δ_y are displacements in the x and y directions respectively (m); a_x and a_y are accelerations in the x and y directions respectively (m/s^2); δ_{lim} = annual limit displacements; and a_{lim} = annual limit accelerations. In this study, δ_{lim}, for 1-year return period, assumes the value of H/1700, based on NBR 6118 [31] and Corelhano et al. [32], and H/1370 based on Huang et al. [33], being H the total height of the building. The term a_{lim}, for 1-year return period, is worth 0.084 m/s^2, recommended by ISO 10137 [34] for residences, and 0.048 m/s^2 based on NBR 6123 [25].

In reality, the displacement limit recommended in [33] is H/400, referring to the designed structural lifetime, around 50 years, while the acceleration limit presented in [25] is 0.1 m/s^2 for 10-year return period. Approximate conversion of these limit criteria to annual return period was made, resulting in the approximately equivalent limits of H/1370 and 0.048 m/s^2, respectively. The conversion applied considers Equations 11 and 12 [25]:

$$S_3 = 0.54 \left[-\frac{\ln(1 - P_m)}{m} \right]^{-0.157} \tag{11}$$

$$F_a = 0.613 \, C_a \, A_e \, (S_1 S_2 S_3 V_0)^2 \tag{12}$$

being S_3 = statistical factor; V_0 = basic wind speed (m/s); $P_m = 0.63$ = probability of V_0 being equaled or exceeded; m = return period (years); F_a = drag force (N); C_a = drag coefficient; A_e = effective frontal area (m^2); S_1 = topographic factor; and S_2 = exposure factor.

Calculating wind forces for return periods of 1 and 50 years, with the same terrain and structure characteristics, the relation $F_{a(1 year)} \cong 0.292 F_{a(50 years)}$ was found. Considering linear behavior of the building, the approximate conversion of the limit criterion of [33] was admitted with the determined relation. The approximate conversion of the limit acceleration of [25] was analogous, differentiated by the return period and in the complementary application of Equation 13 [25], which associates displacements and accelerations:

$$a = (2\pi f)^2 \delta \tag{13}$$

where a = acceleration (m/s^2); f = natural frequency (Hz); and δ = displacement (m).

Returning to the reliability analysis procedures, having random variables $x's$, each one associated to an approved probability density function, and having defined the limit state functions, it was possible to determine the probabilities of failure P_f's by computing the integral of $f_X(x)$ in the failure domain for each situation associated to the limit state functions, according to Equation 14:

$$P_f = P\left[G(X) \le 0\right] = \int_{G(X) \le 0} f_X(x)\, dx \tag{14}$$

where $f_X(x)$ = probability density function for the random variable x of dynamic response.

From the probabilities of failure P_f's, each reliability index β was calculated. Considering the cumulative distribution function of the standardized normal distribution ϕ, one relates β to P_f by Equation 15 (EN 1990 [35]):

$$P_f = \phi(-\beta) \tag{15}$$

In this research, for reliability analysis regarding accelerations, i.e., reversible SLS (serviceability limit states), the annual target reliability index $\beta_1 = 1.28$ ($P_f = 0.10$) was considered as mentioned by Ellingwood [36] *apud* Melchers and Beck [37], because in these cases the analysis is related to the discomfort of the building's occupants, thus reversible damage. For the analysis regarding displacements, i.e., irreversible SLS, $\beta_1 = 1.7$ ($P_f = 0.045$) was adopted in accordance with JCSS [38], as this type of analysis is associated with permanent damage, such as cracking in nonstructural walls.

3 RESULTS AND DISCUSSIONS

The quantity of 5 to 7 points was used in the procedures for estimating the parameters of the regression curves for β, while for the maximums 7 points were applied. This varied quantity is because the cases that failed the goodness-of-fit tests for distribution were disregarded from the regression procedures, justifying the reduced intervals of some regression curves and the absence of others in the presented graphs. Failed intermediate points had their values estimated by the own curves generated with the remaining points. Only regression curves that met the criterion $R^2 \ge 0.8$ were presented.

It is worth mentioning that this study only presents results at the top referring to the x and y directions. Results in the x direction, perpendicular to the largest facade as per Figure 3, for CAARC orientation angles θ of 0° and 90°, presented in the graphs, refer to the longitudinal and transverse responses, respectively, in relation to the wind direction. Similarly, angles θ of 0° and 90° refer to the transverse and longitudinal responses, respectively, for graphs regarding the responses in the y direction, perpendicular to the smallest facade.

In the legends of the charts, the isolated CAARC structure is represented by ISOL, the situations with presence of neighbor at the locations 3b and 6b are called A1 and A2, respectively, and V0 indicates that the largest neighbor facade is perpendicular to the wind direction, while V90 indicates that the smallest neighbor facade is perpendicular to the wind, all according to Figure 3. β_1 represents the annual target reliability index. On equations of the tables, the CAARC orientation angle ranges from $0° \le \theta \le 90°$.

3.1 Accelerations at the top of the CAARC – x-direction

Figure 6 shows, relative to the ISOL curve, how the maximum accelerations increase in the x direction in the presence of neighbor, for any angle θ, and for both neighbor positions and directions. The curves show varying trends in behavior. Table 1 shows the corresponding regression equations. The trend curve A1V0 was a passed exception with $R^2 = 0.79$.
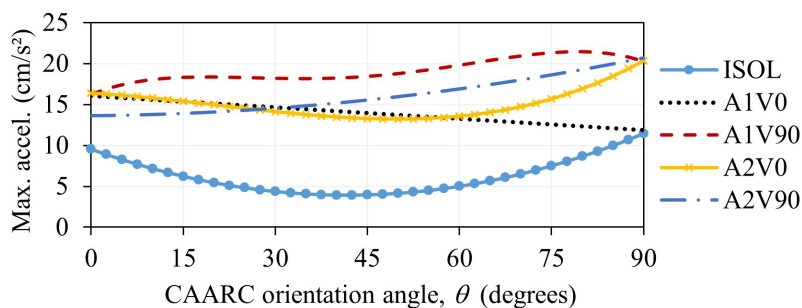

Figure 6. Maximum acceleration at the top of the CAARC, x-direction.

Table 1. Equations for maximum acceleration at the top, x-direction.

Case	Equation (a in cm/s^2, θ in degrees)
ISOL	$a = 0.003322649466\theta^2 - 0.269202026333\theta + 9.54217009588$
A1V0	$a = -0.046263940092\theta + 16.02953714301$
A1V90	$a = -0.00000145621\theta^4 + 0.00025747093\theta^3 - 0.014208078033\theta^2 + 0.299852269828\theta + 16.19668396384$
A2V0	$a = 0.00003492672\theta^3 - 0.002196079150\theta^2 - 0.041165263060\theta + 16.38529763276$
A2V90	$a = 0.000802527850\theta^2 + 0.006644701930\theta + 13.60346271728$

Figure 7 presents reliability indexes for accelerations in the x direction associated with the limit criterion of 8.4 cm/s^2 and the equations for the cases are shown in Table 2. The isolated building presents higher values of β, which is expected because of its lower values of maximum accelerations. Situations with a neighborhood have lower values with good difference, in general, from the isolated case. It appears that most situations are above the target index β_1, in which only cases A2V0 and A2V90 appear below β_1 for higher CAARC orientation angles.
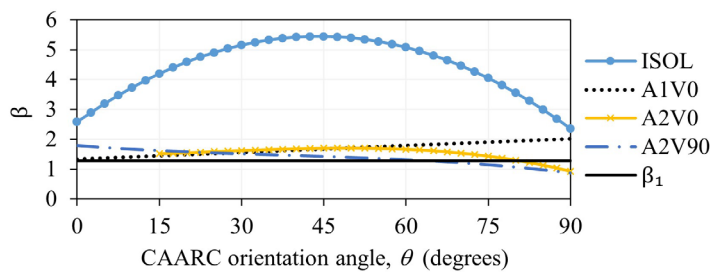

Figure 7. Reliability index β for acceleration, x-direction – limit criterion of 8.4 cm/s^2.

Table 2. Equations of β for acceleration at the top, x-direction – limit criterion of 8.4 cm/s^2.

Case	Equation (θ in degrees)
ISOL	$\beta = -0.00146932996\theta^2 + 0.12981266711\theta + 2.57205262632$
A1V0	$\beta = 0.007652779967\theta + 1.32789105421$
A2V0[(1)]	$\beta = -0.000004141194\theta^3 + 0.000312170082\theta^2 - 0.000574720170\theta + 1.46658837097$
A2V90	$\beta = -0.00000201249\theta^3 + 0.000223160620\theta^2 - 0.014017251870\theta + 1.78606764811$

[(1)] $15° \leq \theta \leq 90°$

Figure 8 shows the indices β relative to the accelerations occurring in the x direction for the limit criterion of 4.8 cm/s^2, and the corresponding equations are in Table 3. Among the situations presented, only those in the case with isolated building (ISOL) for angles θ above a little more than 0° to values close to 90° are above β_1. Like the results for 8.4 cm/s^2 limit, for the isolated case, higher reliabilities occur for the CAARC rotated around 45°. Furthermore, in the presence of neighbor A2 the reliability for transverse accelerations decreases, independent of neighbor angle, compared to ISOL and A1V0.
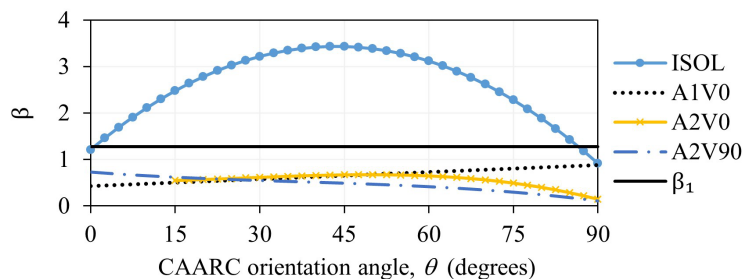

Figure 8. Reliability index β for acceleration, x-direction – limit criterion of 4.8 cm/s^2.

Rev. IBRACON Estrut. Mater., vol. 15, no. 5, e15507, 2022

9/16

Table 3. Equations of β for acceleration at the top, x-direction – limit criterion of 4.8 cm/s^2.

Case	Equation (θ in degrees)
ISOL	$\beta = -0.00116980962\theta^2 + 0.101991725999\theta + 1.21195486620$
A1V0	$\beta = 0.00503726202\theta + 0.42494395416$
A2V0[1]	$\beta = -0.00000289633\theta^3 + 0.000226483840\theta^2 - 0.00110330946\theta + 0.52415107267$
A2V90	$\beta = -0.00000137478\theta^3 + 0.000150406641\theta^2 - 0.009298459007\theta + 0.72788265401$

[1] $15° \leq \theta \leq 90°$

3.2 Displacements at the top of the CAARC – x-direction

It can be seen in Figure 9 that the curve of maximum displacements in the x direction for the isolated structure crosses the other curves, unlike the case of maximum accelerations in the same direction. The longitudinal maximum displacement for ISOL is the largest, while the transverse one is lower, above only the case A1V0. The equations for maximum displacements are shown in Table 4.
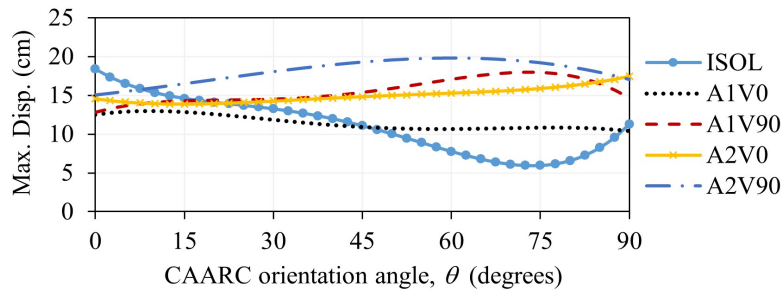

Figure 9. Maximum displacement at the top of the CAARC, x-direction.

Table 4. Equations for maximum displacement at the top, x-direction.

Case	Equation (δ in cm, θ in degrees)
ISOL	$\delta = 0.00000243750\theta^4 - 0.000380843391\theta^3 + 0.018715231350\theta^2 - 0.455191445610\theta + 18.37256570311$
A1V0	$\delta = -0.00000067949\theta^4 + 0.000131312267\theta^3 - 0.007833753050\theta^2 + 0.113335115000\theta + 12.49661161527$
A1V90	$\delta = -0.00000147515\theta^4 + 0.000229091710\theta^3 - 0.010844277100\theta^2 + 0.216225527060\theta + 12.78190492008$
A2V0	$\delta = 0.00000046673\theta^4 - 0.00085156020\theta^3 + 0.005457164050\theta^2 - 0.109778729930\theta + 14.55982880157$
A2V90	$\delta = -0.000020241170\theta^3 + 0.001128587340\theta^2 + 0.084584393890\theta + 15.06308462402$

Reliability indices for displacements in the x direction referring to the H/1370 criterion and their equations are shown in Figure 10 and Table 5, respectively.
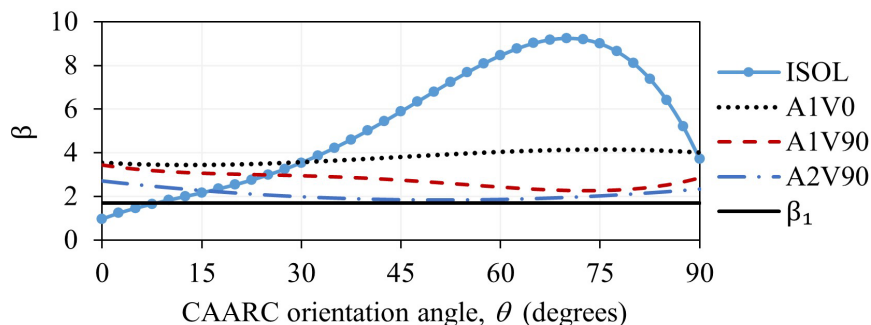

Figure 10. Reliability index β for displacement, x-direction – limit criterion of H/1370.

Figure 10 shows that among A1 cases, the A1V90 showed lower reliabilities, both longitudinally and transversely, especially in the latter. Only the ISOL case for CAARC orientation angle less than or equal to approximately 7.5° appears below the target index β_l.

Table 5. Equations of β for displacement at the top, x-direction – limit criterion of H/1370.

Case	Equation (θ in degrees)
ISOL	$\beta = -0.00000125618\theta^4 + 0.000152025900\theta^3 - 0.00446868431\theta^2 + 0.117015513070\theta + 0.96288728480$
A1V0	$\beta = -0.00005588237\theta^3 + 0.000780020016\theta^2 - 0.017406135000\theta + 3.53397070912$
A1V90	$\beta = 0.00000025354\theta^4 - 0.000039678430\theta^3 + 0.001958352880\theta^2 - 0.046233556840\theta + 3.43464839690$
A2V90	$\beta = 0.000332798690\theta^2 - 0.034058889070\theta + 2.70661547010$

Figure 11 shows curves of the indices β for displacement in the x direction for H/1700 limit. In these curves, as well as in Figure 10, it is noticed the lowest reliability in ISOL for longitudinal displacement, indicating wind protection effect in the presence of neighbor, while in the transverse direction, the presence of neighbor in A1V90 and A2V90 cause a drop in the index, compared to ISOL. In the same figures, in the V90 cases, the presence of the most distant neighbor resulted in lower reliabilities, for all angles θ. Table 6 shows the equations of the curves presented in Figure 11, in which the β indices of the ISOL cases for angles θ less than or equal to approximately 32° are below β_l, as well as much of the A2V90.
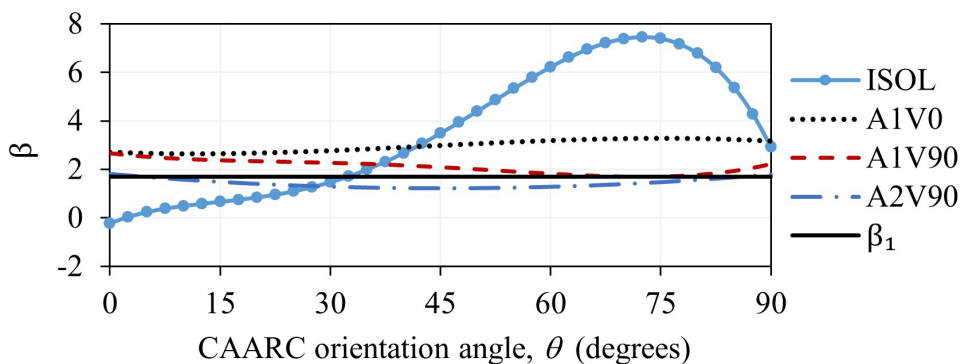

Figure 11. Reliability index β for displacement, x-direction – limit criterion of H/1700.

Table 6. Equations of β for displacement at the top, x-direction – limit criterion of H/1700.

Case	Equation (θ in degrees)
ISOL	$\beta = -0.00001472410\theta^4 + 0.000196441770\theta^3 - 0.00670360239\theta^2 + 0.120479974680\theta - 0.22333710494$
A1V0	$\beta = -0.000004834110\theta^3 + 0.000630037490\theta^2 - 0.012571250320\theta + 2.71007876232$
A1V90	$\beta = 0.000000205610\theta^4 - 0.000031456560\theta^3 + 0.001505978790\theta^2 - 0.035561223500\theta + 2.65208371951$
A2V90	$\beta = 0.000286011070\theta^2 - 0.025916741540\theta + 1.80221515335$

3.3 Accelerations at the top of the CAARC – y-direction

Maximum accelerations at the top of the CAARC for y direction are presented in Figure 12 and the associated equations listed in Table 7. The transverse maximum accelerations are greater than the longitudinal ones for each respective case, similar in general to what was seen for x direction, as well as the ISOL curve values are smaller for all angles θ. Moreover, for almost all these angles, the A1V90 case shows higher maximum accelerations.
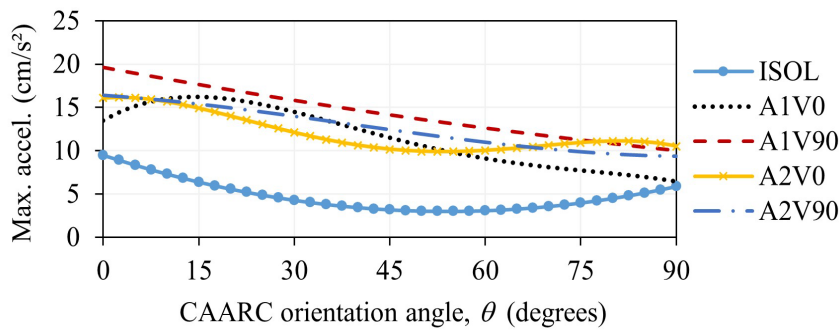
Figure 12. Maximum acceleration at the top of the CAARC, y-direction.

Table 7. Equations for maximum acceleration at the top, y-direction.

Case	Equation (a in cm/s^2, θ in degrees)
ISOL	$a = 0.002225690047\theta^2 - 0.24056270368\theta + 9.50862110886$
A1V0	$a = -0.000001137870\theta^4 + 0.00026116579\theta^3 - 0.019892673670\theta^2 + 0.42605230345\theta + 13.46045121722$
A1V90	$a = 0.000335905550\theta^2 - 0.137000811810\theta + 19.64238985631$
A2V0	$a = -0.00000135470\theta^4 + 0.000248078100\theta^3 - 0.012737366360\theta^2 + 0.062569349320\theta + 16.09125482850$
A2V90	$a = 0.00001211953\theta^3 - 0.001412793870\theta^2 - 0.049432980110\theta + 16.39962882958$

Indices β and their equations are shown in Figure 13 and Table 8, respectively, associated with the acceleration in the y direction for criterion of 8.4 cm/s^2. For the presented ranges of θ, there is only a small part of A1V90 that does not meet the annual target reliability index. In general, a large difference in reliability values is noticed when comparing the case of isolated CAARC with situations in the presence of a neighbor.
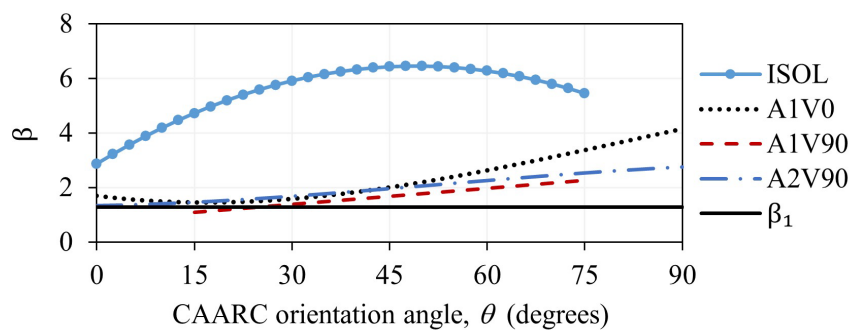

Figure 13. Reliability index β for acceleration, y-direction – limit criterion of 8.4 cm/s^2.

Table 8. Equations of β for acceleration at the top, y-direction – limit criterion of 8.4 cm/s^2.

Case	Equation (θ in degrees)
ISOL[1]	$\beta = -0.00148794428\theta^2 + 0.146050193240\theta + 2.86294662412$
A1V0	$\beta = -0.00000422909\theta^3 + 0.001024846130\theta^2 - 0.030739333480\theta + 1.69813484928$
A1V90[2]	$\beta = 0.019467390500\theta + 0.79398583193$
A2V90	$\beta = -0.000001947930\theta^3 + 0.000305431110\theta^2 + 0.004121794870\theta + 1.32500676872$

[1] $0° \leq \theta \leq 75°$. [2] $15° \leq \theta \leq 75°$.

Regarding reliabilities related to acceleration in the y direction for the limit of 4.8 cm/s^2, considering the same previous cases and ranges of θ, the entire ISOL curve, a small part of A2V90 and A1V0 for θ greater than or equal to

approximately 60° lie above the value of β_l. The presented cases with neighborhood for lower values of θ appear below the target index with some difference. It was noticeable that the variation of the neighbor angle affects the reliability in the A1 neighbor cases, and in the V90 cases the reliability was lower for the presence of the nearest neighbor, as in Figure 13.

3.4 Displacements at the top of the CAARC – y-direction

Figure 14 and Table 9 present, respectively, maximum displacements in the y direction and the associated equations. The trends with neighborhood point to relatively inverse behavior compared to ISOL. Transversely, the maximum displacements increase for the cases A2 studied and A1V90, compared to ISOL, but decrease for A1V0, as well as in the x direction. Longitudinally, the largest maximum displacement is for the isolated CAARC, denoting that the neighborhood causes wind protection effect, which also occurs in the x direction.
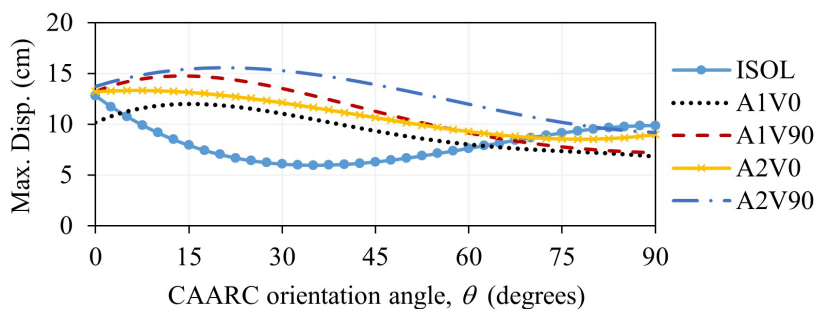

Figure 14. Maximum displacement at the top of the CAARC, y-direction.

Table 9. Equations for maximum displacement at the top, y-direction.

Case	Equation (δ in cm, θ in degrees)
ISOL	$\delta = -0.00004675523\theta^3 + 0.008798984493\theta^2 - 0.44558762299\theta + 12.78382700288$
A1V0	$\delta = -0.00000070265\theta^4 + 0.000161958885\theta^3 - 0.012321855548\theta^2 + 0.27197840024\theta + 10.15315397798$
A1V90	$\delta = -0.00000045184\theta^4 + 0.000125007320\theta^3 - 0.010993252610\theta^2 + 0.238970506570\theta + 13.22239123740$
A2V0	$\delta = 0.000026585790\theta^3 - 0.003369904040\theta^2 + 0.040998381910\theta + 13.20726296445$
A2V90	$\delta = 0.000033214770\theta^3 - 0.005692166290\theta^2 + 0.192839466970\theta + 13.72313240713$

Indices β and their equations, associated with displacements in the y direction for H/1370 criterion, are displayed in Figure 15 and Table 10, respectively. All curves presented are above the annual target reliability index β_l. In general, the drop in reliability is noticeable from A1V0 to A1V90, as well as from A1V90 to A2V90. That is, the neighbor angle and distance influence the dynamic response. Considering the same cases and ranges of θ, for H/1700 criterion, despite even lower indices β, all cases presented indices with values above the target index, like the previous criterion.
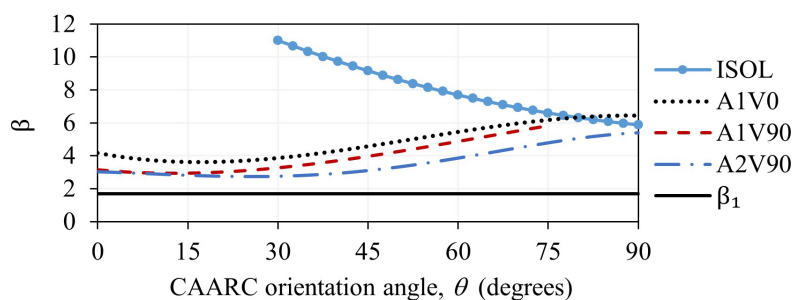

Figure 15. Reliability index β for displacement, y-direction – limit criterion of H/1370.

Rev. IBRACON Estrut. Mater., vol. 15, no. 5, e15507, 2022

13/16

Table 10. Equations of β for displacement at the top, y-direction – H/1370 limit criterion.

Case	Equation (θ in degrees)
ISOL[1]	$\beta = 0.000833927715\theta^2 - 0.18528235305\theta + 15.79946291693$
A1V0	$\beta = -0.00015541544\theta^3 + 0.002442016647\theta^2 - 0.069664402140\theta + 4.16622278539$
A1V90[2]	$\beta = -0.00000800179\theta^3 + 0.001543541115\theta^2 - 0.03515541278\theta + 3.13810043460$
A2V90	$\beta = -0.00000020455\theta^4 + 0.000030969120\theta^3 - 0.000730883140\theta^2 - 0.009533369294\theta + 3.01199256773$

[1] $30° \leq \theta \leq 90°$. [2] $0° \leq \theta \leq 75°$.

4 CONCLUSIONS

It is evident that the presence of neighborhood affects the dynamic responses. In terms of accelerations, the isolated CAARC resulted in lower maximum values, as well as higher reliabilities, for any orientation angle, in both x and y directions. The highest accelerations were in the A1V90 case, in general, as well as the lowest β-indexes in the y direction.

Regarding the displacements, there was the intersection of curves of the isolated case with the other curves, in terms of maximums, reliabilities in the x direction and in some cases in the y direction, as the CAARC was rotated. The isolated case presented the highest maximum displacements of the directions longitudinal to the wind and close to it, in addition to lower reliabilities associated with the x direction, indicating a wind protection effect due to the neighborhood, especially when closer (A1). Compared to the cases with neighbor, the isolated structure showed the smallest maximum displacements in the x direction when oriented at 47° to just under 90°, and in the y direction when oriented from 5° to 60°. The A2V90 case showed larger displacements and lower associated reliability, in general.

Considering the β reliability indexes, for accelerations associated with the ISO 10137 [34] criteria, it was found that for the x direction most situations were found above the target index β_l, in which only the cases A2V0 and A2V90 appeared below β_l for higher CAARC orientation angles, while for the y direction only a small part of A1V90 did not meet the target reliability index, for the presented ranges of θ. Regarding the limit of NBR 6123 [25], for the x direction, among the situations presented, only those in the case with isolated building (ISOL) for angles θ above a little more than 0° up to values close to 90° were found above β_l, while for the y direction the entire ISOL curve, a small part of A2V90 and A1V0 for θ greater than or equal to approximately 60° were situated above the value of β_l.

As for the reliability for displacements, relative to the Huang et al. [33] criterion, in the x direction only the ISOL case for CAARC orientation angle less than or equal to approximately 7.5° appeared below the target index, and for the y direction all the presented curves were above the annual target reliability index β_l. Associated with the limit of NBR 6118 [31], in the x direction the β indices of the ISOL cases for θ angles less than or equal to approximately 32° were found below β_l, as do a good part of A2V90, while in the y direction all the shown curves presented indexes with values above the target index.

There are cases with neighborhood where the highest maxima and lowest reliabilities were found when CAARC was rotated between 0° and 90°. The increase in transverse dynamic responses with respect to wind direction in the presence of a neighborhood is due to the regular vortex shedding. It was observed that a change in the position or angle of the neighbor can influence the reduction of the reliability index. The trends and equations found for the maximums and reliability curves were mostly nonlinear. The probability distribution functions of wind-induced accelerations and displacements, at the top of the building for x and y directions, agreed with the normal distribution, in general.

It is interesting to mention that NBR 6123 [25] is under review and a new section about wind comfort in buildings will be included into this standard.

In further investigations, it would be convenient to perform additional experimental tests for more CAARC orientation angles, thus obtaining more records to determine regression curves, for neighborhoods with other angles and positions, as well as for configurations with more than one neighbor simultaneously. It would also be useful to repeat the tests of the cases that failed the goodness-of-fit tests for distribution in this study. Furthermore, it would be interesting to consider as random variables in the system, for instance, the properties of the building (mass, damping, stiffness, etc.) or more other variables.

Rev. IBRACON Estrut. Mater., vol. 15, no. 5, e15507, 2022

14/16

REFERENCES

[1] P. A. Mendis, T. Ngo, N. Haritos, A. Hira, B. Samali, and J. C. K. Cheung, "Wind loading on tall buildings," *Electron. J. Struct. Eng.*, no. special issue: loading on structures, pp. 41-54, 2007. Accessed: Sept. 11, 2020. [Online]. Available: http://www.ejse.org/Archives/Fulltext/2007/Special/200704.pdf

[2] A. Barile, L. S. Bastos, and J. G. S. Silva, "Human comfort assessment of buildings subjected to nondeterministic wind dynamic loadings," *Rev. IBRACON Estrut. Mater.*, vol. 13, no. 4, pp. e13402, 2020, http://dx.doi.org/10.1590/S1983-41952020000400002.

[3] R. Bashor, S. Bobby, T. Kijewski-Correa, and A. Kareem, "Full scale performance evaluation of tall buildings under wind," *J. Wind Eng. Ind. Aerodyn.*, vol. 104-106, pp. 88–97, May 2012, http://dx.doi.org/10.1016/j.jweia.2012.04.007.

[4] V. C. Rist and S. Svensson, "Methodology for preliminary design of high-rise buildings," M.S. thesis, Dept. Construct. Sci., Lund Univ., Lund, Scania, Sweden, 2016.

[5] L. S. Tapajós, J. A. T. Ferreira, A. F. Lima Neto, M. R. Teixeira, and M. P. Ferreira, "Effect of wind in the design of reinforced concrete buildings," *Rev. IBRACON Estrut. Mater.*, vol. 9, no. 6, pp. 883–910, Dec 2016, http://dx.doi.org/10.1590/S1983-41952016000600005.

[6] S. M. Lamb, K. C. S. Kwok, and D. Walton, "A longitudinal field study of the effects of wind-induced building motion on occupant wellbeing and work performance," *J. Wind Eng. Ind. Aerodyn.*, vol. 133, pp. 39–51, Jul 2014, http://dx.doi.org/10.1016/j.jweia.2014.07.008.

[7] K. C. S. Kwok, P. A. Hitchcock, and M. D. Burton, "Perception of vibration and occupant comfort in wind-excited tall building," *J. Wind Eng. Ind. Aerodyn.*, vol. 97, no. 7-8, pp. 368–380, Sep/Oct 2009., http://dx.doi.org/10.1016/j.jweia.2009.05.006.

[8] M. Burton, K. C. S. Kwok, and A. Abdelrazaq, ""Wind-induced motion of tall buildings: Design for occupant comfort," *Int*," *J. High-Rise Bldg*, vol. 4, no. 1, pp. 1–8, Mar 2015.

[9] S. Lamb and K. C. S. Kwok, "The fundamental human response to wind-induced building motion," *J. Wind Eng. Ind. Aerodyn.*, vol. 165, pp. 79–85, Jun 2017, http://dx.doi.org/10.1016/j.jweia.2017.03.002.

[10] J. Blessmann, "Buffeting effects on neighbouring tall buildings," *J. Wind Eng. Ind. Aerodyn.*, vol. 18, no. 1, pp. 105–110, Feb 1985, http://dx.doi.org/10.1016/0167-6105(85)90077-7.

[11] J. Blessmann, "Neighbouring wind effects on two tall buildings," *J. Wind Eng. Ind. Aerodyn.*, vol. 42, no. 1-3, pp. 1041-1052, Oct. 1992, https://doi.org/10.1016/0167-6105(92)90111-M

[12] J. Blessmann and J. D. Riera, "Interaction effects in neighbouring tall buildings," in *Wind Engineering: Proc. Fifth Int. Conf.*, J. E. Cermak, Ed. New York, NY, USA, 1980, pp. 381-395.

[13] J. Blessmann and J. D. Riera, "Wind excitation of neighbouring tall buildings," *J. Wind Eng. Ind. Aerodyn.*, vol. 18, no. 1, pp. 91–103, Feb 1985, http://dx.doi.org/10.1016/0167-6105(85)90076-5.

[14] X. F. Yu, Z. N. Xie, J. B. Zhu, and M. Gu, "Interference effects on wind pressure distribution between two high-rise buildings," *J. Wind Eng. Ind. Aerodyn.*, vol. 142, pp. 188–197, Jul 2015, http://dx.doi.org/10.1016/j.jweia.2015.04.008.

[15] Y. Hui, Y. Tamura, A. Yoshida, and H. Kikychi, "Pressure and flow field investigation of interference effects on external pressures between high-rise buildings," *J. Wind Eng. Ind. Aerodyn.*, vol. 115, pp. 150–161, Apr 2013., http://dx.doi.org/10.1016/j.jweia.2013.01.012.

[16] P. C. C. N. O Fontoura, "Estudo experimental em túnel de vento dos efeitos de vizinhança em edifícios altos," Ph.D. dissertation, Dept. Civ. Envr. Eng., Univ. Brasília, Brasília, DF, Brazil, 2014.

[17] W. Kim, Y. Tamura, A. Yoshida, and J.-H. Yi, "Interference effects of an adjacent tall building with various sizes on local wind forces acting on a tall building," *Adv. Struct. Eng.*, vol. 21, no. 10, pp. 1469–1481, Jul 2018, http://dx.doi.org/10.1177/1369433217750170.

[18] W. Kim, Y. Tamura, and A. Yoshida, "Interference effects on aerodynamic wind forces between two buildings," *J. Wind Eng. Ind. Aerodyn.*, vol. 147, pp. 186–201, Dec 2015, http://dx.doi.org/10.1016/j.jweia.2015.10.009.

[19] G. S. Vieira, J. L. V. de Brito, and A. M. Loredo-Souza, "Experimental study of the neighborhood effects on the mean wind loading over two equivalent high-rise buildings," *Lat. Am. J. Solids Struct.*, vol. 15, no. 3, pp. e21, May 2018, http://dx.doi.org/10.1590/1679-78253560.

[20] G. S. Vieira, J. L. V. de Brito, and A. M. Loredo-Souza, "Experimental study on the interference intensity produced by the presence of neighboring buildings in the wind action in a tall building," *Rev. IBRACON Estrut. Mater.*, vol. 11, no. 5, pp. 1036–1052, Oct 2018, http://dx.doi.org/10.1590/s1983-41952018000500008.

[21] T. F. A. Lavôr, "Avaliação dos efeitos de martelamento do vento em edifícios altos com vizinhança," Ph.D. dissertation qualifying exam, Dept. Civ. Envr. Eng., Univ. Brasília, Brasília, DF, 2019.

[22] M. A. Smith and L. A. Caracoglia, "Monte Carlo based method for the dynamic fragility analysis of tall buildings under turbulent wind loading," *Eng. Struct.*, vol. 33, no. 2, pp. 410–420, Feb 2011, http://dx.doi.org/10.1016/j.engstruct.2010.10.024.

[23] L. M. Ferreira, A. S. Nowak, and M. K. El Debs, "Development of truck weight limits for concrete bridges using reliability theory," *Rev. IBRACON Estrut. Mater.*, vol. 1, no. 4, pp. 421–450, Dec 2008, http://dx.doi.org/10.1590/S1983-41952008000400005.

[24] J. C. Pantoja, "Geração automática via otimização topológica e avaliação de segurança de modelos de bielas e tirantes," Ph.D dissertation, Dept. Civ. Eng., PUC-Rio, Rio de Janeiro, RJ, 2012.

[25] Associação Brasileira de Normas Técnicas, *Forças Devidas ao Vento em Edificações*, ABNT NBR 6123, 1988.

[26] J. Blessmann, *O Vento na Engenharia Estrutural*, 1st ed. Porto Alegre, Brasil: UFRGS, 1995.

[27] W. H. Melbourne, "Comparison of measurements on the CAARC Standard Tall Building model in simulated model wind flows," *J. Wind Eng. Ind. Aerodyn.*, vol. 6, no. 1-2, pp. 73–88, Jul 1980., http://dx.doi.org/10.1016/0167-6105(80)90023-9.

[28] F. C. Sartori, "Uma comparação de métodos para avaliar a resposta dinâmica de edifícios altos em túnel de vento," M.S. thesis, Civil Eng. Postgraduate Program, Fed. Univ. Rio Grande do Sul, Porto Alegre, Brasil, 2010.

[29] R. W. Clough and J. Penzien, *Dynamics of Structures*, 3rd ed. Berkeley, CA, USA: Comput. Struct., Inc., 2003.

[30] A. G. Davenport, "Note on the distribution of the largest value of a random function with application to gust loading," *Proc.- Inst. Civ. Eng.*, vol. 28, pp. 187–196, 1964., http://dx.doi.org/10.1680/iicep.1964.10112.

[31] Associação Brasileira de Normas Técnicas, *Projeto de Estruturas de Concreto - Procedimento,* ABNT NBR 6118, 2014.

[32] A. G. B. Corelhano, M. R. S. Corrêa, and A. T. Beck, "Reliability of buildings in service limit state for maximum horizontal displacements," *Rev. IBRACON Estrut. Mater.*, vol. 5, no. 1, pp. 84–103, Feb 2012, https://doi.org/10.1590/S1983-41952012000100007

[33] M. F. Huang, C. M. Chan, and K. C. S. Kwok, "Occupant confort evaluation and wind-induced serviceability design optimization of tall buildings," *Wind Struct. Int. J.*, vol. 14, no. 6, pp. 559–582, Nov 2011., http://dx.doi.org/10.12989/was.2011.14.6.559.

[34] International Organization for Standardization, *Bases for Design of Structures – Serviceability of Buildings and Walkways against Vibration*, ISO 10137:2007(E), 2007.

[35] European Committee for Standardization, *Eurocode – Basis of Structural Design,* EN 1990:2002+A1:2005(E), 2002.

[36] B. Ellingwood, "Probability-based loading criteria for codified design," in *4th Intl. Conf. Appl. Statist. Probability Soil Strl. Eng.*, G. Augusti, A. Borri, and G. Vannuchi, Eds. 1983, pp. 237-248.

[37] R. E. Melchers and A. T. Beck, *Structural Reliability Analysis and Prediction*, 3rd ed. Hoboken, NJ, USA: Wiley, 2018.

[38] Joint Committee on Structural Safety, *Probabilistic Model Code Part 1 – Basis of Design 12th Draft*, 2001.

Editor: Sergio Hampshire C. Santos, Guilherme Aris Parsekian.

Rev. IBRACON Estrut. Mater., vol. 15, no. 5, e15507, 2022

16/16